한국동력기계공학회지 제4권 제2호 pp. 17~24 2000년 5월

Fully Developed Turbulent Flow in Roughened Concentric Annuli : Experiment and Analysis

거친환형관내의 완전히 발달된 난류유동 : 실험과 해석

S. W. Ahn

안 수 환

Key Words : Turbulent Fluid Flow(난류유동), Surface Roughness(표면거칠기), Concentric Annulus (동심환형관), Friction Factor(마찰계수), Roughness Position (거칠기위치)

요 약 : 직경비가 0.26, 0.39, 그리고 0.56인 경우 거칠기를 내벽면에, 외벽면에, 그리고 양벽면에 각각 설치한 동심환형관에서 완전히 발달된 난류유동에 대한 거칠기 효과를 실험과 이론으로 해석하였다. 그리고 거칠기 효과를 정량적으로 파악하기 위해 양벽면 모두 매끈한 환형관의 경우도 포함하였다. 실험에서 마찰계수를 구하는데 필요한 속도분포와 전단응력들은 피토튜브와 X-형 열선풍속계를 사용하였다. 이론 해석은 수정대수 난류모델을 사용하였고 그 결과를 이론값과 비교하여 아래의 결론을 얻었다. 1) 무디다이어그램 (Moody diagram)은 거칠기가 설치된 이중관에는 적용할 수 없음을 보였다. 2) 경우 (c) 와 (d)에서는 반경비가 클수록 반드시 마찰계수가 증가하지 않았다. 3) 4개의 경우중 거칠기로 인해 마찰계수가 증가하는 크기의 순서는 경우(d)가 가장 컸고 경우(a)가 가장 작았다.

Nomenclature (see Fig. 1)

C	constant
De	equivalent diameter
f	friction factor
F	normalized friction factor, f_r/f_s
K	von Kârman's constant
P	pitch of roughness elements
R_j^+	$R_j(\tau_{Ro}/\rho)^{0.5}/\nu$
S	$R_o - R_i$
u_j^+	$u_j/(\tau_{Ro}/\rho)^{0.5}$
y_j^+	$y_j(\tau_{Ro}/\rho)^{0.5}/\nu$
Z_{rj}	imaginary location where $u_j = 0$
α	radius ratio, R_i/R_o
δ_j	$\lvert R_m - R_j \rvert$
Δ	δ_j^+/R_j^+
ε	roughness height, eddy diffusivity
ζ_j	y_j^+/δ_j^+

Subscripts:

i	inner
j	i or o
m	corresponding to the location of maximum velocity
M	momentum
o	outer
r	rough
R	radius
s	at sublayer boundary; smooth
t	turbulent

접수일 : 2000년 2월 10일

안수환 : 경상대학교 수송기계공학부

1. Introduction

Our knowledge of the structure of the turbulent fluid flow through channels is based almost exclusively on the experimental results for the turbulent fluid flow through circular tubes and between parallel plates. Such fluid flows are very special cases of channel flows, because these two particular flow channels generate a symmetric velocity profiles, and therefore the positions of the zero shear stress and the maximum velocity coincide. However, the annular channel fluid flows of practical

importance in the heat exchanger system generally have more complex boundary conditions. In these non-circular channels, the velocity profiles are asymmetric, and therefore the position of the zero shear stress is not coincident with the position of the maximum velocity.

For this reason, it has attracted the attention of researchers in the hope that its analysis would resolve some of the evident difference between these two basic flow situations, i.e., symmetrical and asymmetrical flows. Accordingly, Brighton[1] for the first time published the experimental results on the turbulence intensities in three directions, and on the radial shear stress in smooth annuli. Brighton assumed that the positions of the zero shear stress and of the maximum velocity coincided, which has been shown to be untrue[2]. Garimella and Christensen[3] have presented the results of a comprehensive study of the pressure drop in concentric annuli with spirally fluted inner tubes for the laminar, transition, and turbulent flow regimes. And heat transfer and friction factors in the rough annuli with square rib have also been discussed[4-7]. In the present study, the effect of artificial roughness elements and their positions on the turbulent fluid flow in concentric annuli is presented.

2. Analysis

Because of the roughness on the wall and the geometrical characteristic of the annulus, the local flow mechanism in the vicinity of the wall may not satisfy any universal velocity profiles. The large size of the roughness may cause a flow recirculation in the wake zone of the roughness elements and the annulus would have an asymmetric fluid flow. Therefore, the governing equations are divided into the inner and the outer sides from the zero shear stress position. For the analysis, the following assumptions are made:

1. For the smooth wall region, the eddy diffusivity by van Driest[8] for the sublayer,

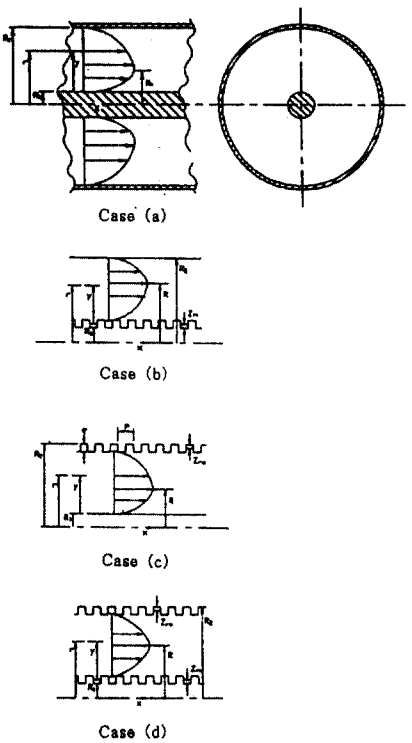

Fig. 1 Idealized model

and that of Reichardt[9] for the fully turbulent region are used.

2. For the values of Z_{rj} in the modified Prandtl mixing length theory, those obtained from the experimental study are used.

2.1 Velocity Distribution

For the velocity distributions, the concept of eddy diffusivity, ε_M is applied. The basic equations governing the transport of the momentum in the annulus can thus be written as:

$$\frac{\tau_j}{\rho} = (\nu+\varepsilon_M)_j \frac{\partial u_j}{\partial y_j} \tag{1}$$

From Eq. (1), the velocity gradients for Case (a) shown in Fig. 1, i. e., both walls smooth, can be shown as follows:

$$\frac{\partial u_i^+}{\partial \zeta_i} = \delta_i^+ \frac{\tau_i/\tau_{Ri}}{1+(\varepsilon_M/\nu)_i} \frac{\tau_{Ri}}{\tau_{Ro}} \quad (0 \le \zeta_i \le 1) \tag{2}$$

$$\frac{\partial u_o^+}{\partial \zeta_o} = \delta_o^+ \left[\frac{\tau_o/\tau_{Ro}}{1+(\varepsilon_M/\nu)_o}\right] \quad (0 \le \zeta_o \le 1) \tag{3}$$

The velocity gradients for the rough side are also given as:

$$\frac{\partial u_i^+}{\partial \zeta_i} = \frac{u_{\tau_{Ri}}}{u_{\tau_{Ro}}} \frac{1}{k_i \zeta_i} \quad (\frac{Z_{ri}^+}{\delta_i^+} \le \zeta_i \le 1) \tag{4}$$

$$\frac{\partial u_o^+}{\partial \zeta_o} = \frac{1}{k_o \zeta_o} \quad (\frac{Z_{ro}^+}{\delta_o^+} \le \zeta_o \le 1) \tag{5}$$

For Case (b) of Fig. 1, i. e., roughness elements on the inner wall only:

$$Z_{ri} = y_m \exp\left[-\frac{\tau_{Ro}}{\tau_{Ri}} [\ln(S - y_{mr}) u_{\tau_{Ro}}/\nu + Ck_o] \right] \tag{6}$$

From the present experimental study, the value of y_m is obtained as:

$$y_m = 0.299S(2.167 - 2.65X10^{-6}Re)(\frac{S}{\varepsilon})^{0.14}[-1.035(\frac{P}{S})^2 + 1.21(P/S) + 0.508](-4.61\alpha^2 + 4.61\alpha - 0.108) \tag{7}$$

For Case (c) of Fig. 1, i. e., the roughness elements on the outer wall only:

$$Z_{ro} = y_m \exp[-\frac{u_{\tau_i}}{u_{\tau_o}} [\ln[R_o(1-\alpha) - y_m] \frac{u_{\tau_i}}{u_{\tau_o}} + Ck_i]] \tag{8}$$

From the present experimental study

$$y_m = 0.299S \cdot Re^{0.066}(S/\varepsilon)^{0.14}(P/S)^{0.201}(1.09\alpha^2 - 0.433\alpha + 0.619) \tag{9}$$

For Case (d), i. e., the roughness elements on both walls, are the same as the given for Cases (b) and (c).

2.2 Eddy diffusivity for momentum, ε_M

Accurate description for the eddy diffusivity for momentum across the flow channel is required for the velocity profiles. Since the assumption of an eddy diffusivity of zero at the center-line in the flow channel is not realistic, we postulate that Reichardt's expression[9] for the eddy diffusivity of momentum can be applicable to the entire turbulent flow regions on the outer smooth wall region of the concentric annulus with proper modification for the region remote from the outer wall. Thus, in dimensionless parameters, the eddy diffusivities can be given as:

For the smooth wall;

$$(\varepsilon_M/\nu)_{it} = (k_i\delta_i^+/6)[1-(y_i^+/\delta_i^+)^2][1+2(1-y_i^+/\delta_i^+)^2]\frac{u_{\tau Ri}}{u_{\tau Ro}} \quad (y_{isub}^+ \le y_i^+ \le \delta_i^+) \tag{10}$$

$$(\varepsilon_M/\nu)_{ot} = (k_o\delta_o^+/6)[1-(y_o^+/\delta_o^+)^2][1+2(1-y_o^+/\delta_o^+)^2] \quad (y_{osub}^+ \le y_o^+ \le \delta_o^+) \tag{11}$$

For the region very close to the smooth wall, the van Driest's dimensionless expression[8] for the eddy diffusivity is used:

$$(\varepsilon_M/\nu)_{jsub} = k_j^2 y_j^{+2}[1-\exp(-y_j^+/A_j^+)]^2 \left| \frac{\partial u_j^+}{\partial y_j^+} \right| \quad (0 \le y_j^+ \le y_{jsub}^+) \tag{12}$$

For the rough region, the Prandtl mixing length theory is employed:

$$(\varepsilon_M/\nu)_j = k_j^2 y_j^{+2} \left| \partial u_j^+/\partial y_j^+ \right| \quad (Z_{rj}^+ \le y_i^+ \le \delta_i^+) \tag{13}$$

Now that the eddy diffusivities (ε_M/ν) are known for the entire fluid region, the velocity profile can be derived. The Reynolds number and friction factor can be obtained in the usual way. Reynolds number is defined as:

$$Re = \frac{2u_b(R_o - R_i)}{\nu} = 2u_b^+(R_o^+ - R_i^+) \tag{14}$$

The average velocity, u_b, can be expressed from the definition in dimensionless parameters as:

For Case (a):

$$u_b^+ = \frac{2\alpha\nu}{R_o(1-\alpha^2)}[\delta_i^+ \int_0^1 (1+\Delta_i\zeta_i)u_i^+(\zeta_i)d\zeta_i + \frac{1}{\alpha}\delta_o^+ \int_0^1 (1-\Delta_o\zeta_o)u_o^+(\zeta_o)d\zeta_o] \tag{15}$$

For Case (b):

$$u_b^+ = \frac{\nu}{R_o}(\frac{2\alpha}{1-\alpha^2})[\delta_i^+ \int_{\frac{Z_{ro}}{\delta_i}}^1 (1+\Delta_i\zeta_i^+)u_i^+ d\zeta_i + \frac{1}{\alpha}\delta_o^+ \int_0^1 (1-\Delta_o\zeta_o)u_o^+ d\zeta_o] \tag{16}$$

For Case (c):

$$u_b^+ = \frac{\nu}{R_o}\frac{2}{1-\alpha^2}\left[\delta_o^+\int_{\frac{Z_{ro}}{\delta_o^+}}^{1}\frac{1}{K_o}\ln\left(\delta_o^+\frac{\zeta_o}{Z_{ro}^+}\right)(1-\Delta_o\zeta_o)d\zeta_o + \alpha\delta_i^+\int_0^1 u\ (1+\Delta_i\zeta_i)d\zeta_i\right] \quad (17)$$

For Case(d):

$$u_b^+ = \frac{2\nu\alpha}{R_o(1-\alpha^2)}\left[\delta_i^+\int_{(Z_m/\delta_i^+)}^{1}(1+\Delta_i\zeta_i)u_i^+(\zeta_i)d\zeta_i + \frac{1}{\alpha}\delta_o^+\int_{(Z_m/\delta_o^+)}^{1}(1-\Delta_o\zeta_o)u_o^+(\zeta_o)d\zeta_o\right] \quad (18)$$

Friction factor in a dimensionless form from the usual definition yields:

$$f = \frac{8(1-\alpha)^2[1+\alpha(\tau_{Ri}/\tau_{Ro})]}{(1+\alpha)}(R_o^+/Re)^2 \quad (19)$$

Assuming that the positions of the maximum velocity and the zero shear stress coincide, the shear stress distributions from a force balance become:

For Case (a):

$$\frac{\tau_{Ri}}{\tau_{Ro}} = \frac{R_o}{R_i}\left[\frac{R_m^2-R_i^2}{R_o^2-R_m^2}\right] \quad (20)$$

For Case (b):

$$\frac{\tau_{Ri}}{\tau_{Ro}} = \frac{R_o}{R_i+Z_{ri}}\left[\frac{R_m^2-(R_i+Z_{ri})^2}{R_o^2-R_m^2}\right] \quad (21)$$

For Case (c):

$$\frac{\tau_{Ri}}{\tau_{Ro}} = \frac{R_o-Z_{Ro}}{R_i}\left[\frac{R_m^2-R_i^2}{(R_o-Z_{ro})^2-R_m^2}\right] \quad (22)$$

For Case (d):

$$\frac{\tau_{Ri}}{\tau_{Ro}} = \frac{R_o-Z_{Ro}}{R_i+Z_{ri}}\left[\frac{R_m^2-(R_i+Z_{ri})^2}{(R_o-Z_{ro})^2-R_m^2}\right] \quad (23)$$

While a fixed value of 0.4 for k_o is taken, the values of k_i is to be calculated from the dimensionless velocity profiles obtained from by the experimental program which is described in the following section,

For Case (a):

$$k_i = 0.525-0.2732\alpha+0.089286\alpha^2 \quad (24)$$

For Case (b):

$$k_i = 0.4 \quad (25)$$

For Case (c):

$$k_i = -0.706+6.376\alpha-7.279\alpha^2 \quad (26)$$

For Case (d):

$$k_i = 0.25333+0.31786\alpha+0.0595\alpha^2 \quad (27)$$

From the continuity of the velocities at the location of the maximum velocity ($r = R_m$, or $\zeta_i = \zeta_o = 1$), the maximum dimensionless velocity position becomes:

$$u_{om}^+ = u_{im}^+ \quad (28)$$

3. Experimental studies

The working fluid is chosen as air in atmospheric condition due to purposes of economical construction of test facilities and also availability of information on physical properties. The annular test section consists of core tubes having three different inner diameters and outer having 97 mm inner diameter. Surface roughening of the tube is done by machining rectangular grooves on the tube surface in the transverse direction on a milling machine. The height of grooves(e) is 1.5 mm and the pitch to height ratio (P/e) for the present study is 2. And detailed dimensions are shown in Ahn and Lee's study[10]. The cleaning chamber consists of commercial air filter for heavy duty vehicle. The control of flow rate of air is done with the movable gate located on the side of the blower. Provisions are made for the measurements of velocity distributions and pressure drops. The constant temperature anemometer (Thermo-System, Inc., Model 1054A) in conjunction with a universal waveform analyzer (Model 6000) was used to detect the velocity distributions. The velocity sensor used is Dantec Model 55P61 miniature X-wire probe: tungsten sensor diameter of 5 μm; sensor length of 1.25 mm; yaw angle of $\pm 45^\circ$; sensor separation of 1.0 mm. To allow minimum disturbance of the flow, the smallest size of hot wire probe and probe support was used.

4. Results and discussion

The measurement was made with a X-type hot wire probe. The solid symbols obtained from the smooth annuli of Case (a) are included in Fig. 2 as a reference to check the effect of the position of the roughness elements. For Case (a), the values from three different Reynolds numbers hardly differ from one another. The values of the present for Case (a) are in a very good agreement with the results of Park[11] except for the region close to the wall.

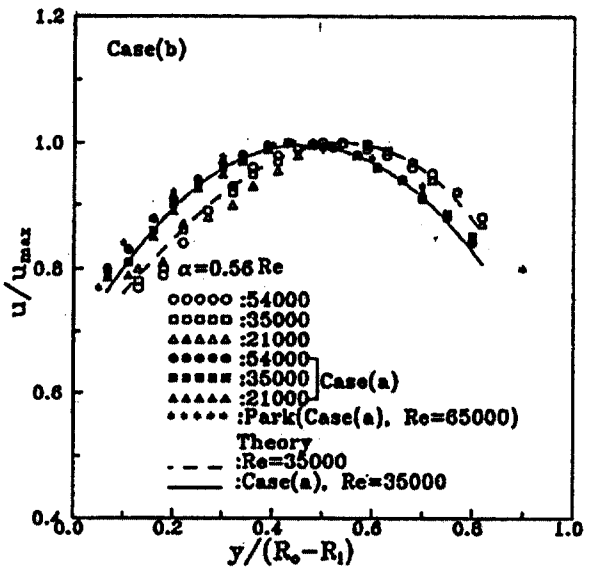

Fig. 2 Velocity profiles

A little deviation at the region close to the wall is attributed to the fact that Park's results (1971) were obtained using pitot tube which may have included the radial fluctuation velocity components. The predicted velocity profiles are compared with the experimental measurements in Fig. 2. In general, the theoretical velocity profiles agree reasonably well with the experimental data, except near the walls. The friction factors, f_i and f_o for the inner and outer regions of an annulus can be defined as:

$$f_i = \frac{\tau_{Ri}}{0.5\rho u_b^2} \tag{29}$$

$$f_o = \frac{\tau_{Ro}}{0.5\rho u_b^2} \tag{30}$$

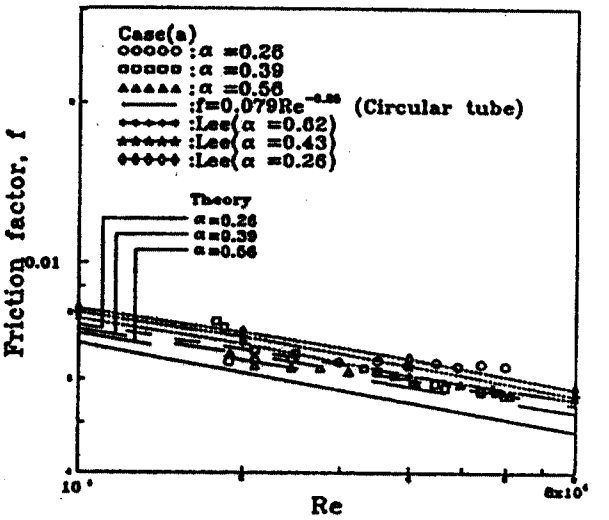

Fig. 3 Friction factors at Case (a)

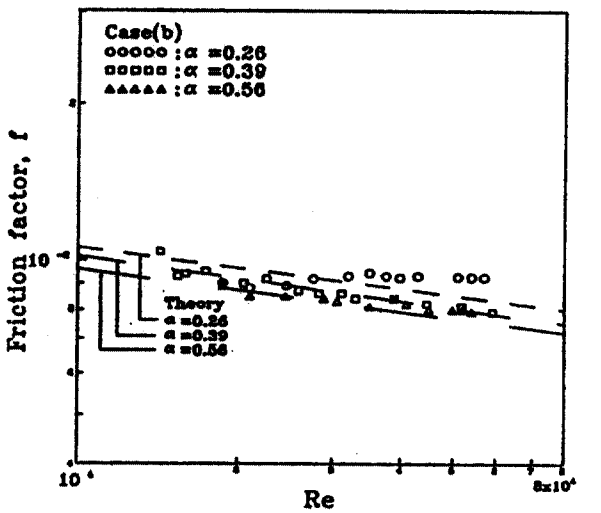

Fig. 4 Friction factors at Case(b)

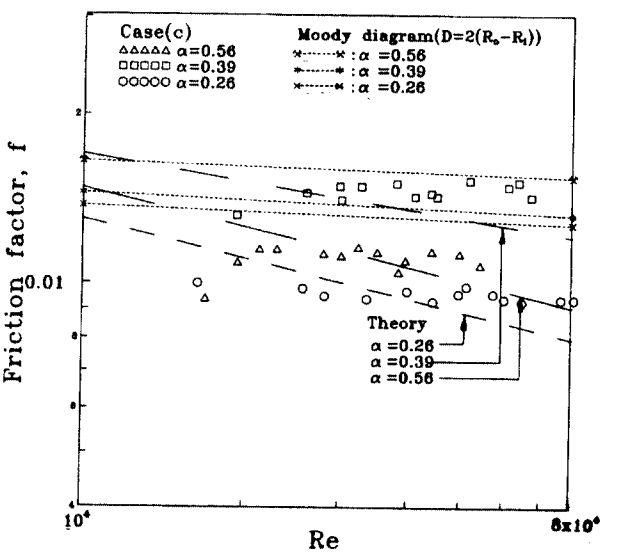

Fig. 5 Friction factors at Case(c)

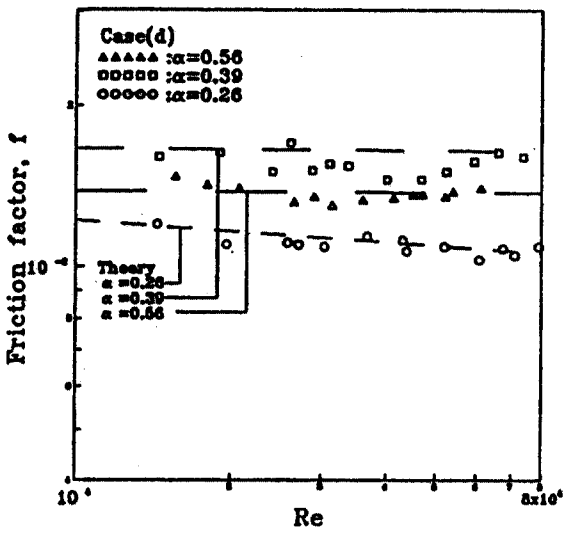

Fig. 6 Friction factors at Case(d)

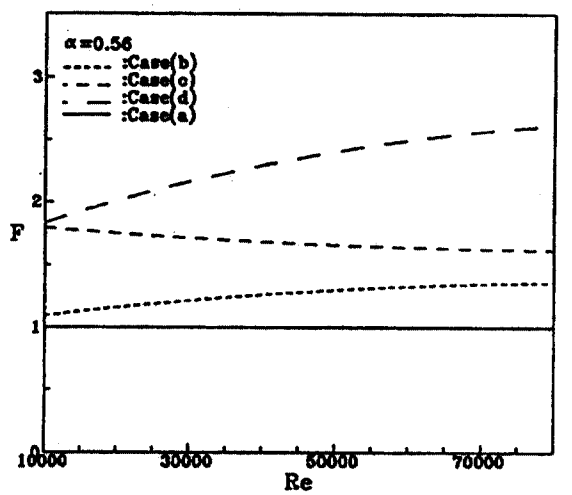

Fig. 7 Normalized friction factors

And the averaged friction factor, f, for the annulus is defined as:

$$f = \frac{R_o f_o + R_i f_i}{R_o + R_i} \qquad (31)$$

Figs. 3 to 6 show the results of the friction factors obtained by the analyses and experiments for the four cases studied, i. e., Cases (a), (b), (c), and (d), respectively. Increase in friction factors can be seen in the order of (a), (b), (c), and (d). This is obvious because the position of the roughness element in the flow passages. For Case (c), the effect of the roughness element on the outer wall is greater than the Case of (b) where the roughness element is on the inner wall. Blasius' data for the smooth circular tube and Lee's results[12] for smooth annuli are included in Fig. 3. The present results for the smooth annuli, Case (a), lie in good agreement with Lee's data[12]. The most interesting feature of the friction factors of the present study can be seen in Cases of (c) and (d) in which it is seen that the higher value of the friction factor is not necessarily associated with the higher value of the radius ratio, α. The value of the friction factor for α = 0.56 is smaller than that of α = 0.39. This is because the relationship between the friction factor defined by Eq. (31) and the Reynolds number defined by Eq. (14) is non-linear. It can seen in Figs. 3 through 6 that the agreement between the analysis and experiment is reasonable. The maximum deviation between two was about 6 %. In Fig. 5, comparison is made with the friction factors taken classical Moody diagram corresponding to the same relative roughness assuming De = D.

The difference, which might be significant in certain critical applications, are due to the following reasons: 1) Though the friction factor depends on velocity, diameter, density, viscosity, roughness, and radius ratio, the Moody diagram predicts a constant friction factor in the Reynolds number considered for the rough side since the flow is completely rough in this region[13]. The present study indicates transition range type flow between the completely smooth and completely rough regimes. This is due to the asymmetry of the roughness distribution on the channel walls. The combination of completely rough flow on the one side and smooth flow on the other in the annulus produces this type of observed behaviour, namely, the variation of total friction with Re, α, S/e, and P/e. 2) The Moody diagram does not recognize the effects of roughness density and radius ratio on the friction factor. For a given S/e and α, the friction factor is same for the given Reynolds number. 3) Also, if the test

channel had different shapes of roughness (i.e, rectangular ribs, triangular ribs, etc.) with the same height, one would still tend to use the same relative roughness value as used above in order to calculate the friction factor from the Moody diagram. This in turn would predict exactly the same friction factor for all of the cases. The problem arises because the Moody diagram is evaluated for a particular type of roughness. To be able to use the Moody diagram, an equivalent sand roughness should also be a function of Reynolds number in the case asymmetric roughness distribution. The use of parameter, Z_{rj} which corresponds to the equivalent sand roughness, is introduced in the present study to provide a step in theoretical analysis of the behaviour of the flow near a wall. In Fig. 7, the increase in friction factor due to the roughness elements, f_r is normalized by the friction factor of the smooth annulus, f_s as:

$$F = f_r/f_s \qquad (32)$$

5. Conclusions

The following conclusions were derived from the analytical and experimental studies made on the friction factor of the fully developed turbulent fluid flow in concentric annuli of the four cases studies:

1) The Moody diagram is not available for the concentric annuli with the surface roughness
2) Increase in friction factors can be seen in the order of (a), (b), (c), and (d) for the four cases studied.
3) The friction factor is not necessarily larger with higher value of the radius ratio for Cases of (c) and (d).

Acknowledgement

This work was supported by the Brain Korea 21 Project

Reference

1. J. B. Brighton, "The Structure of Fully Developed Turbulent Flow in Annuli", Ph. D. Thesis, Purdue University, 1963
2. K. Rehme, "Turbulent Flow in Smooth Concentric Annuli with Small Radius Ratios", J. of Fluid Mechanics, 64, pp. 263~287, 1974
3. S. Garimella and R. N. Christensen, "Heat Transfer and Pressure Drop Characteristics of Spirally Fluted Annuli: Part 1 - Hydrodynamics", Trans. ASME, J. of Heat Transfer, 117, pp. 54~60, 1995,
4. S. W. Ahn, "Friction Factor for Flow in Concentric Annuli with Rib-Roughened Wall", J. of KSME(B), Vol. 23, No. 5, pp. 587~592 (in Korean), 1999
5. S. W. Ahn, "Structure of Turbulence of Fully Developed Flow in Concentric Annuli with Rough Outer Wall", J. of Air-Conditioning and Refrigeration Eng., Vol. 11, No. 1, pp. 1~9 (in Korean), 1999
6. S. W. Ahn and K. C. Kim, "Turbulent Flow in Annuli Depending on the Position of Roughness", J. of KSME(B), Vol. 21, No. 7, pp. 891~899 (in Korean), 1997
7. S. W. Ahn and Y. S. Son, "Turbulent Heat Transfer in Rough Concentric Annuli with Heating Condition of Constant Wall Heat Flux", J. of Korean Society of Marine Eng., Vol. 23, No. 1, pp. 54~61(in Korean), 1999
8. E. R. van Driest, "On Turbulent Flow near a Wall", J. of Aero. Sci., 23, pp. 1007~1112, 1956
9. H. Reichardt, "Vollstandige Darstellung der Turbulenten Geschwindigekeitsverteilung in Glatten Leitungen", ZAMM 31, pp. 208~219, 1951
10. S. W. Ahn and W. J. Lee, "Effect of Roughness Position on the Characteristics of Turbulence in Concentric Annuli", J. of Korean Society for Power System Eng., Vol. 1, pp. 61~69, 1997

11. S. D. Park, "Developing Turbulent Flow in Concentric Annuli: an Analytical and Experimental Study", Ph. D. Thesis, Dpt. of Mech. Eng., University of Ottawa, 1971
12. Y. Lee, "Turbulent Flow and Heat Transfer from the Concentric and Eccentric Annuli", Ph. D. Thesis, Dpt. of Mech. Eng., University of Liverpool, 1964
13. H. Schlinschting, "Experimentelle Untersuchungen zum Rauhigkeitsproblem", Ing. Arch. Vol. 7, pp. 1~34, 1936